Letter

Strain-induced magnetic pattern formation in antiferromagnetic iron borate

T. Janssen [1,2] M. Gidding [1,2] C. S. Davies [1,2] A. V. Kimel [2] and A. Kirilyuk [1,2]

[1]*FELIX Laboratory, Radboud University, Toernooiveld 7, 6525 ED Nijmegen, The Netherlands*

[2]*Radboud University, Institute of Molecules and Materials, Heyendaalseweg 135, 6525 AJ Nijmegen, The Netherlands*

(Received 22 May 2023; accepted 20 September 2023; published 11 October 2023)

Using the crystalline lattice to manipulate magnetic ordering represents an intriguing direction of future research, particularly when attempting to modify the rather robust magnetization of an antiferromagnet (AFM). Here, we study how magnetization can be all-optically rotated in the canted AFM iron borate, utilizing mid- to far-infrared ultrashort light pulses. We discover that this excitation gives rise to a peculiar pattern of metastable magnetic domains with a tunable symmetry, which can be qualitatively understood by considering how light-induced radial strain interacts with the Néel vector. Our results reveal how optically induced strain can be used to spatially modify the magnetic order parameter of an AFM, which could have important applications in future AFM-based data-storage technologies.

DOI: 10.1103/PhysRevB.108.L140405

Our continuously increasing societal dependency on digitally encoded information motivates intense work to make data-storage technologies denser, faster, and less dissipative [1]. Although massive collective efforts have been made by industry to improve the capability of existing devices, we are now approaching the operational limits of conventional data-storage technologies [2]. Therefore, novel and disruptive methods to process and store data are required to meet the ever-increasing demand.

Recently, antiferromagnets (AFMs) have been highlighted as offering a promising basis for advanced spin-based devices and techniques [3]. One of their main advantages lies in the fact that AFMs feature exchange-driven magnetization dynamics that are orders of magnitude faster than the dynamics associated with their ferromagnetic counterparts. AFMs also have a natural robustness to external stimuli, potentially resulting in an extremely stable and highly secure storage medium. Last but not least, the vast majority of magnetic compounds are actually AFMs, which may facilitate much wider material compatibility with existing fabrication processes.

The impervious nature of AFMs, however, makes it very difficult if not impossible to directly manipulate their magnetization with stray magnetic fields. Alternatively, all-optical mechanisms—based on the use of ultrashort laser pulses—can interface directly with antiferromagnetic ordering while arguably offering the fastest possible speeds [4]. While full-scale all-optical switching of order within an AFM has not yet been discovered [5], the direct excitation of terahertz optical phonon modes at resonance has been clearly shown to be capable of temporarily modifying order parameters in a variety of other systems [6–9]. In particular, it was recently demonstrated that the magnetization of iron-garnet films can even be permanently switched by illuminating the ferrimagnet with infrared (IR) optical pulses tuned in frequency to match those of longitudinal optical phonon modes [10]. The central role of strain in the process was unambiguously confirmed by the highly nontrivial spatial distribution of the switched magnetization. From this, an intriguing question arises: how does this mechanism operate and manifest in an AFM?

In this Letter, we explore how optically induced strain can be used to drive magnetization dynamics and pattern formation in an AFM. To circumvent the difficulties normally associated with observing magnetic domains in collinear AFMs, we have opted to study the canted AFM iron borate ($FeBO_3$). The IR pump pulses were provided by the lasers at the free-electron laser (FEL) facility FELIX [11]. We directly observe that the IR excitation generates a peculiar and reproducible domain pattern, consisting of a distribution of circulating magnetization at the center with tapered domains extending outwards along a certain axis. This pattern is rather distinct to that found in iron garnets [10]. We qualitatively explain the origin of this domain pattern in terms of the interaction of the Néel vector with the strain-induced radial anisotropy field.

Iron borate has a rhombohedral calcitelike crystal structure ($R\bar{3}c$ symmetry). The Fe^{3+} ions form two antiferromagnetically coupled sublattices, where the superexchange is mediated by O^{2-} ions. The broken inversion symmetry of the crystal supports the Dzyaloshinskii-Moriya interaction (DMI), which can be described in terms of an effective magnetic field $H_{\mathrm{DMI}} = 61.9\,\mathrm{kOe}$ [12,13]. The latter slightly cants the spins by 1°, resulting in a weak magnetic moment of $4\pi M_s = 115\,\mathrm{G}$ at room temperature.

The spins of the Fe^{3+} ions experience both an easy-plane anisotropy ($H_A = 1.7\,\mathrm{kOe}$) and a very weak hexagonal in-plane anisotropy ($H_{A'} = 0.26\,\mathrm{Oe}$). The DMI-induced net magnetic moment, combined with a strong magneto-optical response in the visible spectral range, allows us to track magnetization dynamics via magneto-optical microscopy. For example, at the wavelength $\lambda = 525\,\mathrm{nm}$, the Faraday rotation is maximum (magnitude of $2300\,^\circ\mathrm{cm}^{-1}$) while the absorption is negligible ($39\,\mathrm{cm}^{-1}$) [14]. Since the magnetic moment of iron borate lies (at equilibrium) within the sample's plane, we tilt the sample slightly with respect to the probe's wave vector, in order to have a magnetization component collinear with the

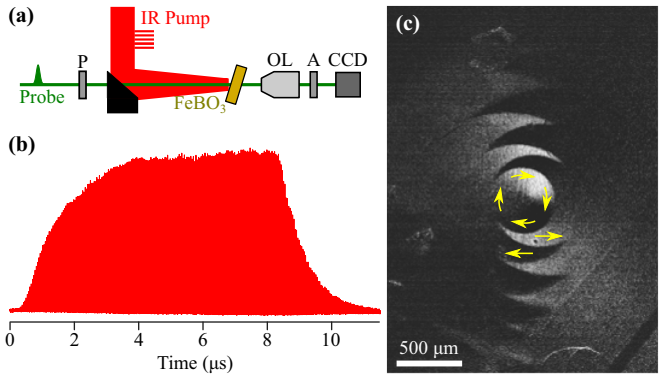

FIG. 1. (a) Sketch of the two-color pump-probe setup. The infrared (IR) pumping macropulse is focused by a parabolic mirror onto the $FeBO_3$ sample (tilted by 17°). The probe pulse, after passing a polarizer (P) and transmitting through $FeBO_3$, is collected by an objective lens (OL), filtered by an analyzer (A), and detected by a charge-coupled device (CCD). (b) Temporal profile of a typical 8-μs-long pumping macropulse, containing ≈ 200 micropulses coming at 25 MHz. (c) Exemplary raw magneto-optical image of the magnetic domain pattern in $FeBO_3$ induced by a single pumping macropulse of wavelength $\lambda = 14.5\,\mu$m. The yellow arrows indicate the orientation of magnetization.

wave vector. This scheme, however, gives rise to a sizable contribution of birefringence [15]. To therefore achieve the best compromise in minimizing this birefringence while maximizing the Faraday rotation, we found that tilting the sample by 17° yielded optimum magneto-optical contrast for both wavelengths of $\lambda = 520$ and 532 nm used for illumination.

The magnetization dynamics of $FeBO_3$ is investigated using a single-shot pump-probe microscopy scheme. The IR pump pulses, delivered by one of the FELs at the FELIX laboratory, come in the form of 8-μs-long bursts (so-called macropulses) at a rate of 10 Hz. Inside each macropulse are micropulses with a temporal separation of 40 ns [see Fig. 1(b)]. Each transform-limited micropulse has a duration of 1–3 ps, with a bandwidth tunable between 0.5 and 2% and a central wavelength tunable between 3 and 100 μm. The macropulse energy was measured to be between 0.6 and 0.85 mJ, leading to a single micropulse energy of ≈4 μJ. The IR pump is focused onto the sample's surface using an off-axis parabolic mirror. The sample's magnetization is probed either by a cw laser ($\lambda = 520$ nm) or synchronized 5-ns-long laser pulses ($\lambda = 532$ nm). By illuminating the sample and/or recording magneto-optical images at different predetermined time delays, we reconstruct the time-resolved dynamics of magnetization.

Prior to excitation, a small magnetic field is used to initialize the sample's magnetization into a single-domain state. After excitation by a single IR macropulse with central wavelength $\lambda = 14.5\,\mu$m, we observe a distinct and peculiar pattern of magnetic domains as shown in Fig. 1. At the center, this pattern consists of circulating magnetization resembling a large magnetic vortex. Extending periodically outwards from the center are tapered domains, physically corresponding to an alternating polarity of the magnetization. A similar magnetic pattern was observed before in as-quenched FeNiSiB

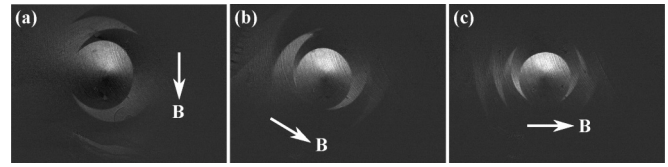

FIG. 2. (a–c) Background-corrected magneto-optical images of the domain pattern, taken after exposing $FeBO_3$ to a single macropulse with an external magnetic field applied ($\mathbf{B} = 0.4$ mT) at different in-plane angles as indicated.

metallic glass [16,17], although that pattern was nucleated and stabilized by a point defect. Here, in contrast, this pattern is dynamically formed by the IR pulse. Moreover, we observe that the tapered magnetic domains are aligned either with the axis of the applied field or, when an external magnetic field is absent, along the axis of the magnetization's initial direction (Fig. 2).

Magnetic vortices are typically found in thin circular or square platelets where the magnetization rotates in plane to minimize the demagnetizing field at the sample edges [18,19]. Helical textures of magnetization can also be found in materials with strong DMI, and magnetic skyrmions have been previously observed in iron borate [20]. However, the size of the vortexlike feature we observe in our sample can exceed diameters of 380 μm which is far too large to be classified as a conventional skyrmion [21,22]. Moreover, taking into account that the velocity of domain walls in iron borate can exceed 14 km/s for relatively small magnetic fields [23], we expected the pattern to relax in just tens of nanoseconds after the arrival of the pumping IR macropulse [24]. Surprisingly, after the initial rapid formation, the nonpropagating pattern remained stable for several milliseconds, eventually relaxing back to its original homogeneous ground state (as shown in Fig. 3). This relaxation process can be considerably accelerated by applying a constant magnetic field. For example, the application of a very weak bias magnetic field 55 μT caused the inhomogeneous pattern to essentially vanish after 4 ms. In the absence of any magnetic field, this decay took more than twice as long.

In contrast, all the timescales related to the formation of the pattern are much shorter than milliseconds. Our time-resolved experiments have shown that the formation of the magnetic domain pattern is certainly faster than the microsecond scale of the macropulse, probably occurring across several nanoseconds based on the requirement for the excited optical phonons to couple and transfer energy to the acoustic phonon modes [25]. In the case considered here, $FeBO_3$ has a wealth of optical phonon modes in the mid- to far-IR spectral range [26–28]. Such optical phonons typically have lifetimes on the order of several picoseconds, presumably leading to a similar lifetime of any optically induced strain. Therefore, the long lifetime and minimal changes in the shape of the domain pattern during the first milliseconds after excitation actually lead to a reasonable argument that the observed magnetic domain pattern represents a metastable state of the system.

The size and orientation of the magnetic domain pattern depend strongly on the strength and direction of the applied external magnetic field. As the strength of the in-plane

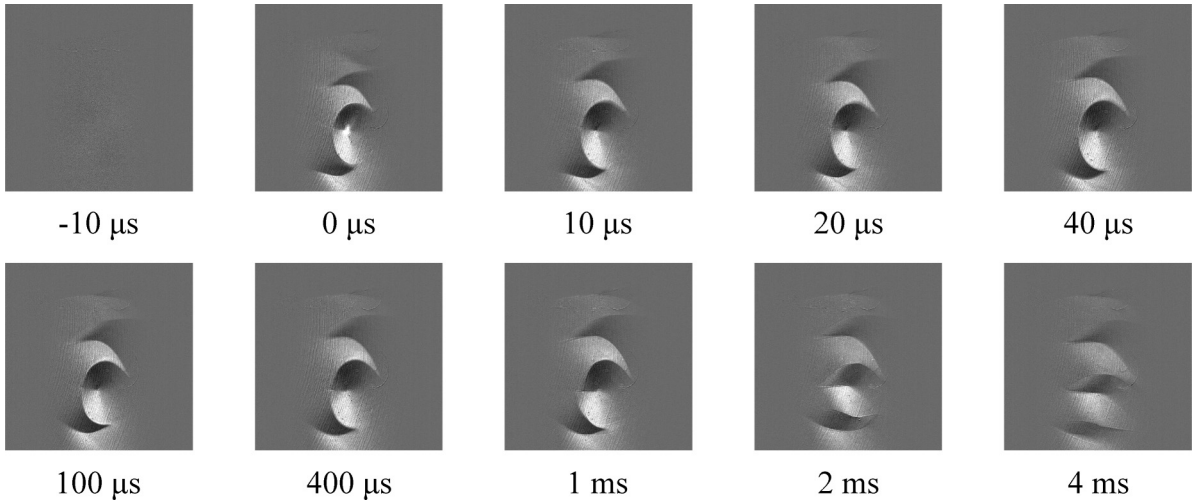

FIG. 3. Temporal evolution of the magnetic domain pattern recorded while applying a constant in-plane magnetic field of strength 55 μT. The visible harmonic of the IR pump pulse can be seen in the center of the image taken at the pump-probe overlap (0 μs).

magnetic field is increased, the magnetic pattern shrinks in size, with more periods of the tapered domains fitting within the fixed field of view. Changing the sign of the magnetic field does not affect the pattern overall, aside from reversing the orientation of the magnetization and the sense of the curling magnetization, which is clear from the inversion of the magneto-optical contrast. The orientation of the domain pattern is solely determined by the orientation of the applied magnetic field. Upon rotating the magnetic field while continuously exposing the sample to macropulses coming at 10 Hz, the pattern freely rotated with the applied magnetic field, showing that it is not bound to any crystallographic axis. If the magnetic field strength exceeds a certain threshold, the pattern does not appear at all, with the sample's magnetization being bound to the applied magnetic field.

To understand how the observed peculiar magnetic domain pattern is formed in the AFM $FeBO_3$, we present a qualitative explanation based on how the Néel vector interacts with strain. A similar line of reasoning can also be used to explain how magnetization can be affected by strain in a ferromagnetic system. Let us begin by considering the latter, which in practice produces a four-domain pattern of switched magnetization as shown in Ref. [10]. We assume that this material has square magnetocrystalline anisotropy, with the x and y axes coinciding with the axes of anisotropy. As a result, the net magnetization M in equilibrium can align in four directions given by these two axes. Before excitation, the magnetization is uniformly aligned along the y axis by a small externally applied magnetic field. The IR pump pulse has a Gaussian distribution of energy, inducing macroscopic deformation with a similarly Gaussian spatial profile [29]. Assuming that the latter is limited to the plane of the film, and taking into account only diagonal components, the magnetoelastic energy is given by

$$E_{\mathrm{ME}} = b_1\left(\epsilon_{xx}m_x^2 + \epsilon_{yy}m_y^2\right) \tag{1}$$

where b_1 is the magnetoelastic coupling coefficient and ϵ_{ii} is the induced strain along the ith axis [30]. Further details of how the IR pulse generates such strain are provided in Ref. [10]. This term gives rise to radially symmetric anisotropy as shown in Fig. 4(b) (black double-headed arrows). Moreover, this transient radial anisotropy is strongest not at the center of the irradiated region but rather where the gradient of the excitation is largest [10,29]. This locus is indicated by the yellow circle in Fig. 4(b).

Along the y axis, the radial strain-induced anisotropy exerts no torque, and so no changes in the magnetization are expected here. In contrast, close to the x axis (orthogonal to the magnetization's initial orientation), the transient anisotropy exerts maximum torque. This gives rise—exactly along the x axis—to an unstable equilibrium, with no obvious direction of torque being exerted on $\mathbf{M}$. Slightly away from the x axis, however, the anisotropy applies a torque with well-defined sign, causing the magnetization to undergo large-amplitude precession either clockwise or anticlockwise in these four quadrants [Fig. 4(c)]. If the cone angle of the magnetization precession is sufficiently large enough, the magnetization close to the x axis can even be stabilized by the uniaxial anisotropy axis coinciding with the x axis. This therefore explains the specific footprint of magnetic switching observed previously in ferrimagnetic iron garnets [10].

Let us now discuss how the same mechanism works in an AFM. The latter comprises two sublattices of magnetization $\mathbf{M}_1$ and $\mathbf{M}_2$ oriented antiparallel to each other albeit with a slight canting. As a result, there is a small net magnetic moment $\mathbf{m} = \mathbf{M}_1 + \mathbf{M}_2$ that is orthogonal to the Néel vector $\boldsymbol{l} = \mathbf{M}_1 - \mathbf{M}_2$, as schematically shown in Fig. 4(a). In an AFM, the Néel vector actually aligns with any uniaxial anisotropy, rather than $\mathbf{m}$. We must emphasize here that our magneto-optical microscopy measurements shown in Figs. 1–3 detect $\mathbf{m}$, allowing us to infer the orientation of $\boldsymbol{l}$.

If we now assume that the IR pulse similarly induces—via strain—radial uniaxial anisotropy in the AFM [10], one can expect a different pattern of magnetic domains. Let us start with assuming the $\boldsymbol{l}$ vector is uniformly oriented parallel to the y axis (and, by extension, $\mathbf{m}$ is uniformly aligned along the x axis). The easy-plane type of anisotropy found in $FeBO_3$ allows the optically induced strain to affect magnetization far beyond the spot at which the IR pump is focused. Similar to the case of the FM, the strain-induced anisotropy cannot

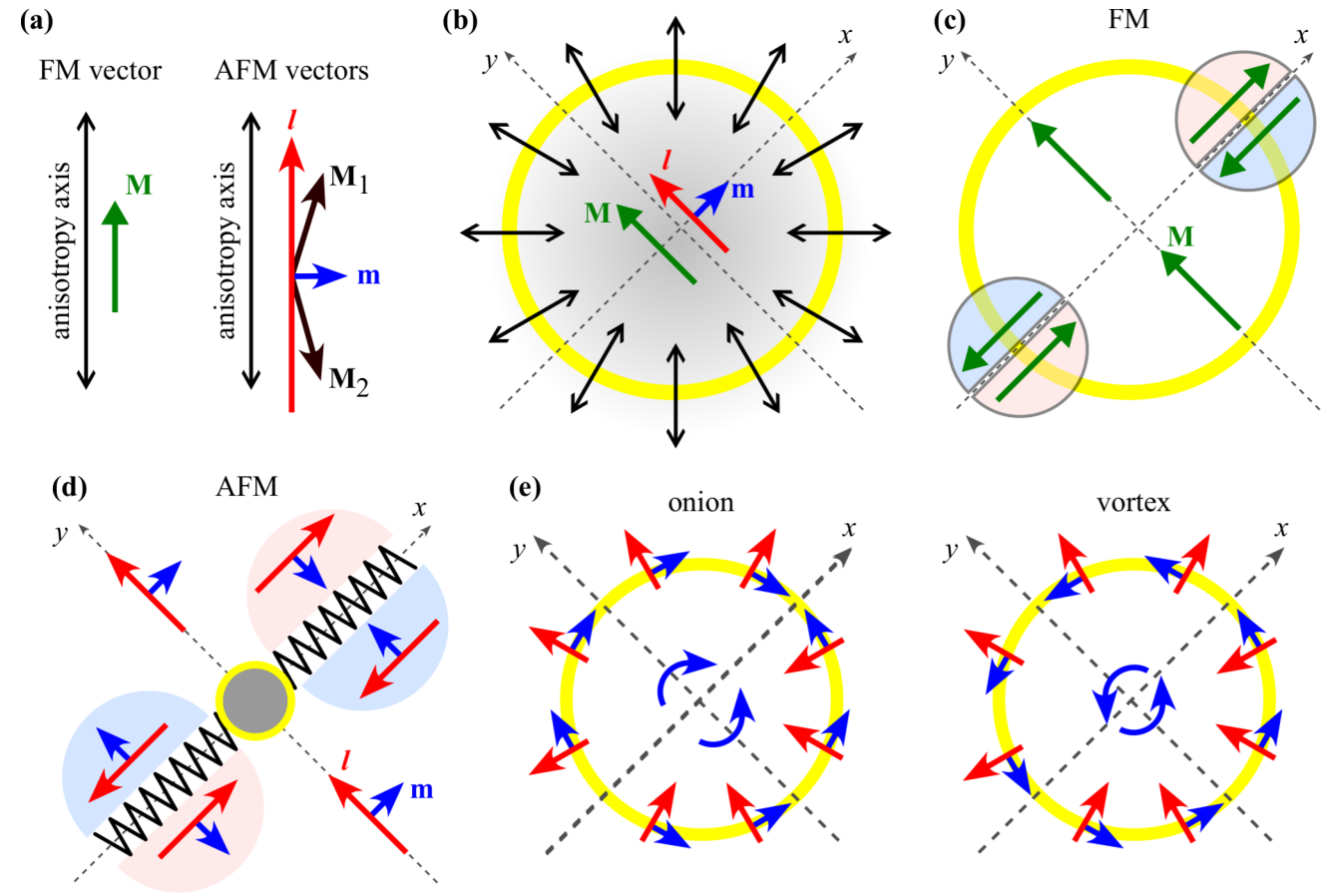

FIG. 4. (a) Schematic of how the magnetization **M** of a ferromagnet (FM) and the Néel vector **l** and magnetization **m** of a canted antiferromagnet (AFM) align with uniaxial anisotropy. (b) Before excitation, the magnetization of the FM or the Néel vector of the AFM is uniformly oriented along the *y* axis. Upon excitation by an infrared pulse, strain gives rise to a radially symmetric distribution of anisotropy (black double-headed arrows), maximized in strength at the locus indicated by the yellow circle. (c), (d) The magnetic domain pattern that emerges as a result of optically induced strain in the FM and AFM respectively. (e) Left: The "onion"-like magnetic configuration that one would expect at the center of the irradiated area. Right: The "vortex"-like domain pattern that is actually observed in our magneto-optical experiments.

exert any torque on the $\boldsymbol{l}$ vector across the line $x = 0$. Just above and below the x axis, in contrast, the transient radial anisotropy exerts maximum torque on $\boldsymbol{l}$, and so the magnetization close to the x axis undergoes substantial rotation, either clockwise or anticlockwise [Fig. 4(d)]. This effect explains why the strain-induced tapered magnetic domains observed in Fig. 2 persistently align with the axis along which the B field is applied. Extending this line of reasoning even further, one can expect a head-to-head or tail-to-tail domain wall to emerge along the x axis. Such a magnetic configuration is energetically unfavorable. Consequently, one can reasonably anticipate that this domain wall fractures to form a zig-zig pattern of magnetic domains. This gives rise to the tapered magnetic domains observed in Figs. 1–3.

At the very center of the irradiated region $x = y = 0$, the radial anisotropy cannot single-handedly perturb **l**. Away from this point, however, one would logically expect the magnetization to kinetically produce the magnetic configuration shown in the left panel of Fig. 4(e). This bidomain pattern, consisting of magnetization with opposite circulation on either side of the central axis, is rather reminiscent of the "onion" configuration previously identified in micromagnetic modeling of rings [31] and disks [32]. Our experimental results, however, instead clearly show the formation of a magnetic vortexlike pattern at the center of the irradiated region [right panel of Fig. 4(e)]. The vortex state is much more energetically favorable compared to the onion state, with the former minimizing the flux closure in the plane of the sample. We therefore speculate that the onionlike state is actually initially formed by the infrared pulse, and this is subsequently transformed into the vortex-like state across a timescale shorter than our experiment's temporal resolution (≈5 ns). To therefore elucidate fully the observed magnetic pattern in $FeBO_3$ and assess the veracity of our presented explanation, further experimental works must explore how the strain-induced magnetization dynamics in $FeBO_3$ evolve across subnanosecond timescales.

In conclusion, we have studied how strain, induced optically using mid- to far-IR optical pulses delivered by a FEL, interacts with the magnetization comprising the canted AFM iron borate. Using magneto-optical microscopy, we have directly observed that the weak magnetic moment at the center of the irradiated spot curls into a vortexlike distribution, while simultaneously forming tapered magnetic domains with periodically reversed orientation along a specific axis.

By exploring the temporal dynamics of the pattern across microsecond to millisecond timescales, and moreover how the pattern depends on the optical parameters and the magnetization's initial orientation, we have revealed that the pattern arguably represents a metastable state of the magnetization across macroscopic length scales. We qualitatively explain how this pattern of magnetic switching forms by considering how the strain-induced radial anisotropy interacts with the Néel vector. This explanation is also consistent in explaining the phononic switching of magnetization found in the ferrimagnetic iron garnet presented in Ref. [10]. Our results not only reveal how the mechanism of phononic switching of magnetization manifests in antiferromagnetic materials, but also show how strain can be used to address magnetic ordering in future spintronic technologies involving AFMs.

The authors thank R. Schäfer for fruitful discussions and all technical staff at FELIX for providing technical support. We acknowledge the Nederlandse Organisatie voor Wetenschappelijk Onderzoek (NWO-I) for their financial contribution, including the support of the FELIX Laboratory and funding via Contract No. 680-91-131. We also acknowledge support from the COST Action Grant No. CA17123 MAGNETOFON.

[1] N. Jones, How to stop data centres from gobbling up the world's electricity, Nature (London) **561**, 163 (2018).
[2] *The International Roadmap for Devices and Systems* (IEEE, Piscataway, NJ, 2020), pp. 1–32, https://irds.ieee.org/images/files/pdf/2020/2020IRDS_MM.pdf.
[3] A. Nordrum, The fight for the future of the disk drive, IEEE Spectrum **56**, 44 (2018).
[4] A. V. Kimel, A. Kirilyuk, A. Tsvetkov, R. V. Pisarev, and T. Rasing, Laser-induced ultrafast spin reorientation in the antiferromagnet $TmFeO_3$, Nature (London) **429**, 850 (2004).
[5] S. Schlauderer, C. Lange, S. Baierl, T. Ebnet, C. P. Schmid, D. Valovcin, A. Zvezdin, A. Kimel, R. Mikhaylovskiy, and R. Huber, Temporal and spectral fingerprints of ultrafast all-coherent spin switching, Nature (London) **569**, 383 (2019).
[6] M. Först, C. Manzoni, S. Kaiser, Y. Tomioka, Y. Tokura, R. Merlin, and A. Cavalleri, Nonlinear phononics as an ultrafast route to lattice control, Nat. Phys. **7**, 854 (2011).
[7] R. Mankowsky, A. Subedi, M. Först, S. O. Mariager, M. Chollet, H. T. Lemke, J. S. Robinson, J. M. Glownia, M. P. Minitti, A. Frano, M. Fechner, N. A. Spaldin, T. Loew, B. Keimer, A. Georges, and A. Cavalleri, Nonlinear lattice dynamics as a basis for enhanced superconductivity in $YBa_2Cu_3O_{6.5}$, Nature (London) **516**, 71 (2014).
[8] R. Mankowsky, M. Först, and A. Cavalleri, Non-equilibrium control of complex solids by nonlinear phononics, Rep. Prog. Phys. **79**, 064503 (2016).
[9] A. S. Disa, M. Fechner, T. F. Nova, B. Liu, M. Först, D. Prabhakara, P. G. Radaelli, and A. Cavelleri, Polarizing an antiferromagnet by optical engineering of the crystal field, Nat. Phys. **16**, 937 (2020).
[10] A. Stupakiewicz, C. S. Davies, K. Szerenos, D. Afanasiev, K. S. Rabinovich, A. V. Boris, A. Caviglia, A. V. Kimel, and A. Kirilyuk, Ultrafast phononic switching of magnetization, Nat. Phys. **17**, 489 (2021).
[11] D. Oepts, A. F. G. van der Meer, and P. W. Amersfoort, The free-electron-laser user facility FELIX, Infrared Phys. Technol. **36**, 297 (1995).
[12] R. Wolfe, A. J. Kurtzig, and R. C. LeCraw, Room-temperature ferromagnetic materials transparent in the visible, J. Appl. Phys. **41**, 1218 (1970).
[13] A. Kalashnikova, Ultrafast light-induced dynamics of spins and lattice in iron oxides, Ph.D. thesis, Radboud University, Nijmegen, 2009.
[14] A. J. Kurtzig, R. Wolfe, R. C. LeCraw, and J. W. Nielsen, Magneto-optical properties of a green room-temperature ferromagnet: $FeBO_3$, Appl. Phys. Lett. **14**, 350 (1969).
[15] D. O. Ignatyeva, A. A. Voronov, P. V. Shilina, P. O. Kapralov, S. V. Yagupov, Y. A. Mogilenec, M. B. Strugatsky, and V. I. Belotelov, Birefringence-mediated enhancement of the magneto-optical activity in anisotropic magnetic crystals, ACS Photonics **9**, 2767 (2022).
[16] W. Rave, R. Schäfer, and A. Hubert, Quantitative observation of magnetic domains with the magneto-optical Kerr effect, J. Magn. Magn. Mater. **65**, 7 (1987).
[17] A. Hubert and R. Schäfer, *Magnetic Domains: The Analysis of Magnetic Microstructures*, 3rd ed. (Springer, New York, 2009).
[18] A. Wachowiak, J. Wiebe, M. Bode, O. Pietzch, M. Morgenstern, and R. Wiesendanger, Direct observation of internal spin structure of magnetic vortex cores, Science **298**, 577 (2002).
[19] A. B. Butenko, A. A. Leonov, A. N. Bogdanov, and U. K. Rößler, Theory of vortex states in magnetic nanodisks with induced Dzyaloshinskii-Moriya interactions, Phys. Rev. B **80**, 134410 (2009).
[20] E. G. Galkina, A. Yu. Galkin, B. A. Ivanov, and F. Nori, Magnetic vortex as a ground state for micron-scale antiferromagnetic samples, Phys. Rev. B **81**, 184413 (2010).
[21] X. S. Wang, H. Y. Yuan, and X. R. Wang, A theory on skyrmion size, Commun. Phys. **1**, 31 (2018).
[22] B. A. Ivanov, Ultrafast spin dynamics and spintronics for ferrimagnets close to the spin compensation point, Low Temp. Phys. **45**, 935 (2019).
[23] V. G. Bar'yakhtar, B. A. Ivanov, and M. V. Chetkin, Dynamics of domain walls in weak ferromagets, Ups. Fiz. Nauk. **146**, 417 (1985).
[24] M. V. Chetkin and A. de la Campa, Maximum velocity of a domain wall in a weak ferromaget, Pis' ma Zh. Eksp. Teor. Fiz. **27**, 168 (1978).
[25] M. Gidding, T. Janssen, C. S. Davies, and A. Kirilyuk, Dynamic self-organisation and pattern formation by magnon-polarons, Nat. Commun. **14**, 2208 (2023).
[26] J. Joubert, T. Shirk, W. White, and R. Roy, Stability, infrared spectrum and magnetic properties of $FeBO_3$, Mater. Res. Bull. **3**, 671 (1968).
[27] K. Wakamura, T. Okuda, and T. Tsushima, Vibrational spectra of antiferromagnetic $FeBO_3$, Opt. Commun. **23**, 249 (1977).

[28] K. Parlinski, J. Łażewski, P. Jochym, A. Chumakov, R. Rüffer, and G. Kresse, Influence of magnetic interaction on lattice dynamics of $FeBO_3$, Europhys. Lett. **56**, 275 (2001).

[29] L. D. Landau and E. M. Lifshitz, *Course of Theoretical Physics* (Elsevier, Amsterdam, 2013).

[30] S. Chikazumi, *Physics of Ferromagnetism* (Oxford University, New York, 1997), Vol. 94.

[31] J. Rothman, M. Kläui, L. Lopez-Diaz, C. A. F. Vaz, A. Bleloch, J. A. C. Bland, Z. Cui, and R. Speaks, Observation of a bi-domain state and nucleation free switching in mesoscopic ring magnets, Phys. Rev. Lett. **86**, 1098 (2001).

[32] J. K. Ha, R. Hertel, and J. Kirschner, Micromagnetic study of magnetic configurations in submicron permalloy disks, Phys. Rev. B **67**, 224432 (2003).